Available online at www.sciencedirect.com
SCIENCE DIRECT®
Journal of Solid State Chemistry 177 (2004) 1513–1519
JOURNAL OF SOLID STATE CHEMISTRY
http://elsevier.com/locate/jssc

Synthesis, properties and structure of ion exchanged hydrosodalite

Emma Kendrick* and Sandra Dann

Chemistry Department, Loughborough University, Loughborough LE11 3TU, UK

Received 17 April 2003; received in revised form 21 August 2003; accepted 8 December 2003

Abstract

Alkali metal and alkali-earth metal hydrosodalites with the formula $M_6[AlSiO_4]_6 \cdot 8H_2O$ (M = Li, Na, K, Mg, Ca, Sr) have been prepared by ion exchange of $Na_6[AlSiO_4]_6 \cdot 8H_2O$ using a solution of the appropriate metal nitrate solution under reflux for a period of 24 h. The starting materials and products were characterized using a combination of techniques including IR, DSC, TGA, ICP, AA, MASNMR and X-ray diffraction. The alkali metal and alkali-earth metal hydrosodalites crystallize with the primitive cubic sodalite unit cell and an ordered AlO_4/SiO_4 framework in the space group $P\bar{4}3n$ with cell parameters lying between 8.8 and 9.2 Å. The structures of these materials have been refined using powder X-ray diffraction data in order to delineate structural changes as a function of the occluded cation. Temperature-dependent powder X-ray diffraction has been used to observe changes in the structure as a function of temperature. Results from the DSC and TGA analysis show that the temperature at which water is lost from the β cages is a two-stage process. In the second stage, the temperature rises as the size of occluded cation increases, implying that the presence of a larger cation in the six-ring window blocks the path of the exiting water molecules.

Keywords: Hydrosodalite; Ion exchange

1. Introduction

Sodalite is a well-known class of anion-containing framework constructed from vertex-linking TO_4 tetrahedra into four- and six-membered rings to form a cage structure. This cage structure is known as the β cage and it is a building block observed in other zeolites such as zeolite A and zeolite X. The general formula for a sodalite is $M_8[TT'O_4]_6A_y \cdot nH_2O$, where M and A are single or divalent cations and anions, respectively. Normally, an anion lies at the center of the cage that is tetrahedrally coordinated to four cations. Anions with different geometries, such as SO_4^{2-} [1–2] and Cl^-, [3], and cations of different sizes, such as potassium [4] and calcium [1], can be incorporated into the sodalite cage by partial collapse of the framework. Partial collapse of the framework is achieved by deviation from perfect TO_4 geometry, the twisting of the TO_4 group by a tilt angle (ϕ) and the deformation of the T–O–T' framework angle (γ) (Fig. 1).

The sodalites can be modified to produce a range of materials with specific properties including cathodochromicity, photochromicity and ion conduction [5]. In order to engineer these specific properties and to understand how they arise, it is necessary to investigate the interactions of the non-framework constituents and the effect of chemical and thermal treatment on the sodalites. This work concentrates on the anionic-free sodalite system, hydrosodalite.

Hydrosodalite, $Na_6[AlSiO_4]_6 \cdot 8H_2O$, [6] is an unusual sodalite-type material because the anion at the center of the cage has been replaced by four water molecules. Therefore, only three sodium ions per cage are required to counterbalance the charge on the aluminosilicate framework. Hydrosodalite crystallizes with a cubic structure in the space group $P\bar{4}3n$ with cell parameter 8.9 Å. The aluminum and silicon atoms are on special sites 6*b* (1/4, 0, 1/2) and 6*c* (1/4, 1/2, 0), respectively, while the oxygen atom in the framework is on a general 24*i* (x, y, z) site.

The structure and properties of silver and thallium hydrosodalite prepared by ion exchange of $Na_6[AlSiO_4]_6 \cdot 8H_2O$ with the appropriate metal nitrate have been reported previously [7]. The hydrosodalite precursor, hydroxysodalite, can be synthesized by two methods; the Hund method [8] and a hydrothermal method using kaolin [9]. In both cases, the anion-free hydrosodalite

*Corresponding author. Fax: +44-1509-223925.
E-mail address: e.kendrick@lboro.ac.uk (E. Kendrick).

0022-4596/$ - see front matter © 2003 Elsevier Inc. All rights reserved.
doi:10.1016/j.jssc.2003.12.008

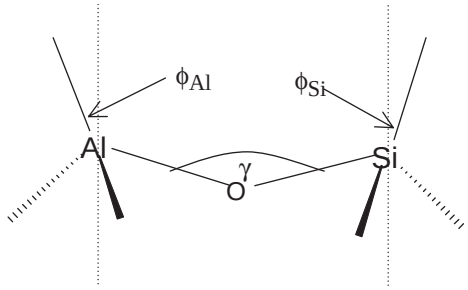

Fig. 1. *T*–O–*T* (γ) and tilt (ϕ) angles in aluminosilicate sodalite structures.

can be prepared by Soxhlet extraction of the host with water. Previous work comparing the lithium and potassium ion exchange of hydrosodalite prepared by both these methods has been reported [10]. This work concentrates on preparing alkali and alkali-earth metal hydrosodalite materials from hydrosodalite prepared from kaolin through ion exchange. Structural parameters derived from Rietveld refinement are reported and correlated with the size of the occluded anion. Temperature-dependent data from in situ X-ray diffraction and thermal analysis are also reported.

2. Experimental

The precursor of hydrosodalite, hydroxysodalite, was synthesized according to the following method. Kaolin and 16 M NaOH were placed in a Parr digestion bomb at 220°C for 24 h [9]. The hydroxysodalite was refluxed in water for 48 h at 110°C to produce hydrosodalite. Ion exchange was performed on hydrosodalite by refluxing in a 2 M solution of the appropriate alkali metal nitrate for 24 h. The cation content was determined using either AA (K^+, Na^+) or ICP (Li^+, Ca^{2+}, Sr^{2+}, Mg^{2+}) spectroscopy. Although complete ion exchange was not achieved after the 24 h period, prolonged and repeated ion exchange did not achieve a higher level of substitution. Powder X-ray diffraction data were collected on all samples using a Bruker D8 powder diffractometer fitted with a PSD detector using monochromatic, Cu$K\alpha_1$ radiation. High-quality X-ray data for Rietveld refinement were collected from 10–100° (2θ) over a period of 12 h using a 0.0147° 2θ step. Rietveld refinement on the diffraction data was performed using the GSAS [11] suite of programs. In situ high-temperature X-ray diffraction was performed on the Li, K, Ca cation exchanged hydrosodalite samples and hydrosodalite, the temperature was raised at 0.5°C/s over a temperature range 27–900°C and X-ray diffraction data were collected over an hour period at 50°C intervals. TGA and DSC were performed on a Mettler TA3000 system and IR measurements were taken using a Paragon IR spectrometer. ^{27}Al and ^{29}Si MASNMR was performed on hydrosodalite and lithium, potassium and calcium ion exchanged hydrosodalites, using a Varian Unity Inova spectrometer and a 5 mm (rotor o.d.) MAS probe.

3. Results

3.1. Structure refinement

Refinement was carried out in the space group $P\bar{4}3n$ using the starting model of hydrosodalite [8] with an ordered framework consisting of AlO_4 and SiO_4 tetrahedra using the programme GSAS. [11] Occupancies of the alkali and alkali-earth metal cations were fixed according to the proportions determined from ICP/AA analysis. Initial stages of the refinement included all the instrumental parameters (background, scale factor and peak shape parameters). The atomic parameters (atomic positions and temperature factors) were then slowly introduced for all atoms. Final atomic parameters are summarized in Table 1 and important bond lengths and angles are given in Table 2. An example of the refinement profile for the lithium-exchanged sample is given in Fig. 2. Due to relatively low ratio of data points to parameters in this refinement, the χ^2 values are in some cases high. However, the wRp values are low and indicate a good closeness of fit. The cell parameters derived from Rietveld refinement and the average size of the occluded cations (as determined by ICP/AA analysis) are correlated in Fig. 3 and indicate that the cell size increases with the average size of the ionic radii.

The prolonged reflux of hydrosodalite in alkali-earth metal nitrate solution caused partial collapse of the β cage and appearance of amorphous material in the X-ray diffraction pattern. The poorer crystallinity of these samples was confirmed by the MASNMR results; vide infra.

3.2. Structure

All hydrosodalite structures were successfully refined in the space group $P\bar{4}3n$ demonstrating an ordering of the aluminum and silicon atoms in the framework. The framework bond lengths (Al–O ≈ 1.7 Å, Si–O ≈ 1.6) are consistent with the literature values for tetrahedral aluminum and silicon and are relatively unaffected by the ion exchange process. The major differences occur around the alkali/alkali-earth cation site where the bond lengths and angles distort to accommodate cations of differing size. In a typical sodalite cage structure, tilting of the tetrahedra in the six-membered ring generates three short and three longer bonding interactions between the framework oxides and the metal cation. In a fully expanded cage where the tetrahedra show no

Table 1
Refined atomic parameters for $M_6[AlSiO_4]_6 \cdot 8H_2O$; e.s.d.'s are given in parentheses

Sample	Al Uiso	Si Uiso	O1 Suiso	O2 Uiso	Na Uiso	Framework oxygen				Water
						O1*x*	O1*y*	O1z	Na*x*	O2*x*
Hydroxy	0.001(3)	0.005(3)	0.007(1)	0.019(1)	0.05(1)	0.1408(6)	0.1505(6)	0.4366(4)	0.1779(3)	
Hydrosod	0.003(2)	0.001(2)	0.0089(7)	0.028(1)	0.0361(9)	0.1383(3)	0.1480(3)	0.4319(2)	0.1568(2)	0.3764(2)
$CsNO_3$ 1	0.003(2)	0.004(2)	0.054(9)	0.024(2)	0.072(2)	0.1371(3)	0.1480(3)	0.4316(2)	0.1502(2)	0.3782(2)
$CsNO_3$ 2	0.007(1)	0.008(1)	0.0125(5)	0.076(1)	0.052(1)	0.1396(2)	0.1487(2)	0.4331(1)	0.1588(1)	0.3844(1)
KNO_3 1	0.006(1)	0.005(1)	0.0136(6)	0.047(2)	0.0430(6)	0.1463(3)	0.1531(3)	0.4675(3)	0.1644(1)	0.3793(2)
KNO_3 2	0.0013(3)	0.012(2)	0.0149(7)	0.099(3)	0.0289(7)	0.1446(3)	0.1526(3)	0.4716(4)	0.1596(2)	0.3734(3)
KOH	0.0035(9)	0.0011(9)	0.0073(5)	0.042(2)	0.0509(6)	0.1459(3)	0.15230(3)	0.4672(3)	0.1659(2)	0.3707(9)
$NaNO_3$	0.0008(2)	0.006(2)	0.0075(6)	0.052(6)	0.00256(8)	0.1446(3)	0.1526(3)	0.4425(2)	0.1708(2)	0.3925(2)
$LiNO_3$ 1	0.023(1)	0.018(1)	0.0268(7)	0.146(2)	0.068(2)	0.1399(2)	0.1473(2)	0.4277(2)	0.1649(3)	0.3903(2)
$LiNO_3$ 2	0.009(1)	0.009(1)	0.0132(6)	0.181(3)	0.063(2)	0.1386(2)	0.1474(2)	0.4286(2)	0.1699(3)	0.3937(2)
$Mg(NO_3)_2$	0.004(2)	0.107(4)	0.007(2)	0.050(4)	0.023(3)	0.1359(5)	0.1586(5)	0.4517(5)	0.1023(5)	0.3627(6)
$Ca(NO_3)_2$	0.016(1)	0.05(1)	0.0242(9)	0.0170(10)	0.042(2)	0.1410(3)	0.1484(3)	0.4301(2)	0.1521(2)	0.3862(2)
$Sr(NO_3)_2$	0.009(2)	0.011(2)	0.056(2)	0.032(3)	0.038(1)	0.1439(6)	0.1556(6)	0.4703(6)	0.1734(2)	0.38890(3)

Table 2
Calculated interactomic distances (Å) and refinement parameters; e.s.d.'s given in parentheses

Sodalite reflux	Na (%)	*M* (%)	w*R*p	χ^2	Cell (Å)	Bond lengths (Å)					*T*–O–*T* (γ)	Tilt angle (deg)	
					a	Al–O	Si–O	Na–O1	Na–O1	Na–O2	Al–O–Si	Al	Si
Hydroxysoalite	100	0	0.048	3.856	8.904(1)	1.636(6)	1.749(6)	2.340(4)	2.3(5)	2.7(5)	136.9(3)	24.2(3)	22.8(3)
$LiNO_3$ 1	62	38	0.039	5.083	8.8381(5)	1.633(3)	1.746(3)	2.439(2)	2.511(2)	3.362(4)	135.21(9)	26.2(1)	24.7(1)
$LiNO_3$ 2	66	34	0.048	9.277	8.7854(5)	1.652(3)	1.736(2)	2.324(2)	2.507(3)	3.430(4)	132.92(8)	27.3(1)	26.2(1)
Hydro	100	0	0.072	39.60	8.7675(3)	1.636(2)	1.737(2)	2.293(2)	2.547(3)	3.399(4)	133.53(8)	27.3(1)	25.9(1)
$NaNO_3$	100	0	0.050	27.49	8.8687(3)	1.646(3)	1.742(3)	2.454(2)	2.622(3)	3.072(2)	138.76(1)	21.7(1)	20.6(1)
KNO_3 1	28	72	0.059	12.40	9.2060(5)	1.626(3)	1.727(3)	2.876(4)	2.670(2)	3.409(5)	152.2(2)	11.0(1)	10.5(1)
KNO_3 2	32	68	0.057	19.73	9.1786(3)	1.638(2)	1.723(3)	2.789(3)	2.678(2)	3.147(3)	149.8(1)	12.7(1)	12.0(1)
KOH	16	84	0.065	24.54	9.1850(2)	1.637(3)	1.726(3)	2.775(3)	2.753(6)	3.257(1)	149.8(1)	12.7(1)	12.1(1)
$CsNO_3$	100	0	0.056	1.955	8.8399(6)	1.627(4)	1.753(4)	2.490(3)	2.431(3)	3.491(4)	135.2(1)	26.5(1)	24.8(1)
$Mg(NO_3)_2$	50	50	0.043	13.87	8.8458(2)	1.636(2)	1.742(2)	2.434(1)	2.487(2)	3.456(2)	135.54(7)	25.6(1)	24.2(1)
$Ca(NO_3)_2$	67	33	0.055	26.05	8.951(3)	1.528(5)	1.802(5)	2.7272(7)	2.191(6)	3.716(8)	143.65(3)	19.5(1)	17.0(1)
$Sr(NO_3)_2$	94	6	0.060	26.07	8.8041(5)	1.649(3)	1.734(3)	2.450(2)	2.389(2)	3.571(3)	133.9(1)	26.4(1)	25.2(1)

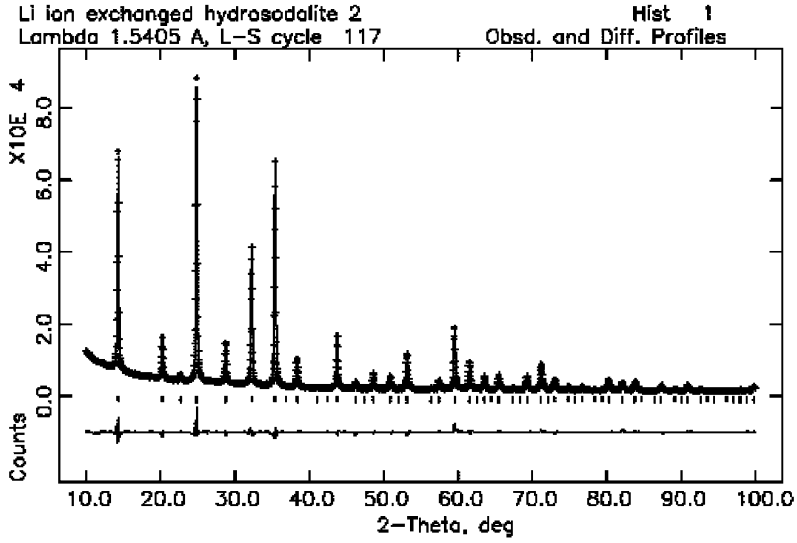

Fig. 2. Rietveld refinement profile of $(Li,Na)_6[AlSiO_4]_6 \cdot 8H_2O$. The upper crossed line represents the experimental data and the upper solid line the calculated pattern. The lower solid line represents the fit.

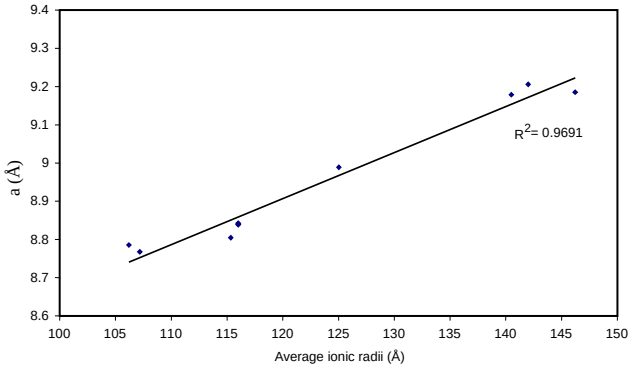

Fig. 3. Correlation of cell parameter (a) with average ionic radius.

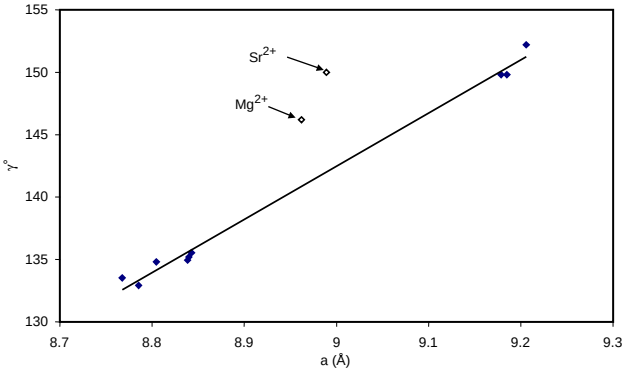

Fig. 5. Change in T–O–T angle (γ) with cell parameter (a).

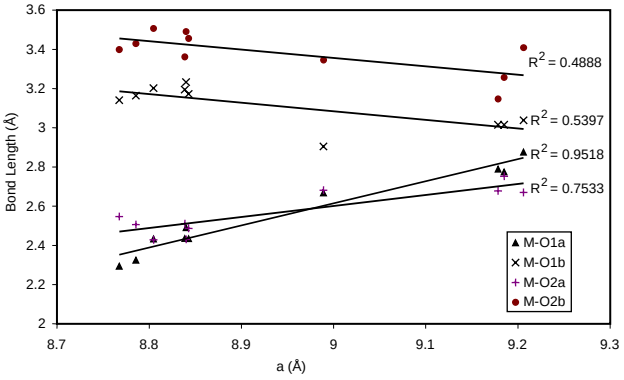

Fig. 4. Change in cation-oxygen bond length with cell parameter (a).

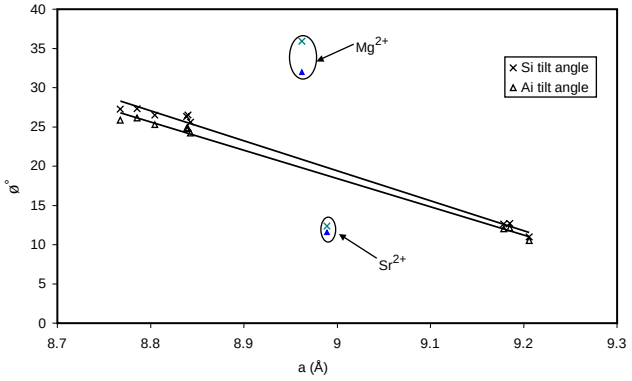

Fig. 6. Change in tilt angle (Φ) with cell parameter (a).

tilt, all six interactions become the same. A further bonding interaction exists in this case between the metal cation and the oxygen from the water molecule. In the case of the lithium-exchanged sample, the shorter cation-framework oxide bond length (M–O1(a)) is 2.324(2)Å, while the longer cation-framework oxide bond length (M–O1(b)) is 3.164(2)Å. As the size of the cage increases, the shorter cation-framework oxide bond length (M–O1(a)) lengthens and the longer cation-framework oxide bond length (M–O1(b)) shortens gradually becoming more similar as the tilt angles get smaller. In contrast, the (M–O2(a)) bond length (from the cation to the oxide ion on the water molecule) is solely governed by the size of the cage and hence increases in size as the cell size increases (Fig. 4).

Figs. 5 and 6 show the correlations between the Al–O–Si (γ) bond angle and the Al/Si tilt angle (ϕ) with the cell parameter, respectively. While the data for the alkali metal cations correlate well with the cell parameters, the data for the alkali-earth metal cations show a much poorer correlation. Since every divalent alkali-earth metal cation replaces two alkali metal cations for charge neutrality, these systems are considerably more disordered than those where the exchanging alkali metal directly replaces another alkali metal cation. It is likely that the atomic position of the divalent cation [1] will not be identical to that of the alkali metal cation, but since ion exchange is not complete it is not possible to model this behavior.

3.3. Thermal behavior

The percentage weight loss determined by TGA indicates that four water molecules per unit cell are lost at low temperature followed by another four water molecules lost per unit cell at higher temperature. Some samples, such as the potassium exchanged materials, have a very low temperature for initial weight loss of about 100°C and due to drying of the samples after ion exchange, a small amount of water has been lost from the system before TGA was performed. The weight changes observed by TGA/DSC are summarized in Table 3. The DSC results show a linear correlation to those derived from TG analysis (Fig. 7). TGA shows as the ionic radii and hence cell parameter increase, the initial water loss occurs at a lower temperature and the second water loss occurs at a higher temperature (Fig. 8). This means for the materials with the smaller unit cells, such as those containing lithium, the two regions coalesce leading to a single temperature range (150–250°C) at which all the water molecules are lost from the sodalite cage. However, for

Table 3
% Mass loss and thermal events observed by TGA/DTA

	TGA % mass loss		TGA temp (°C)		DSC temp (°C)	
	1	2	1	2	1	2
Hydrosodalite	6.61	7.9	108(6)	238(11)	185(7)	309(11)
$CsNO_3$ 1	6.72	6.7	120(6)	245(11)	120(7)	260(11)
$CsNO_3$ 2	6.12	5.9	114(6)	230(11)	160(7)	305(11)
KNO_3 1	6.02	6.6	126(6)	300(11)	140(7)	360(11)
KNO_3 2	6.78	6.2	125(6)	325(11)	135(7)	370(11)
KOH	5.41	8.2	120(6)	350(11)	155(7)	370(11)
$NaNO_3$	5.97	7.6	145(6)	247(11)	182(7)	310(11)
$LiNO_3$ 1	13.2	—	100(6)	150(11)	200(7)	312(11)
$LiNO_3$ 2	11.92	—	200(6)	250(11)	205(7)	330(11)
$Mg(NO_3)_2$	28.36		160(6)	275(11)	167(7)	272(11)
$Ca(NO_3)_2$	7.98	7.8	160(6)	325(11)	175(7)	360(11)
$Sr(NO_3)_2$	10.98	4.1	120(6)	290(11)	185(7)	282(11)

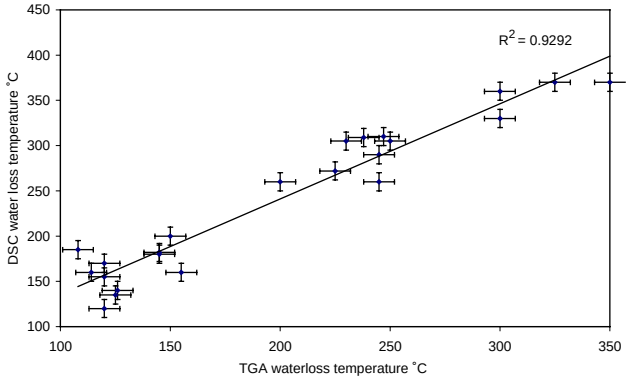

Fig. 7. Correlation between DSC and TGA temperatures of water loss and crystal morphology change.

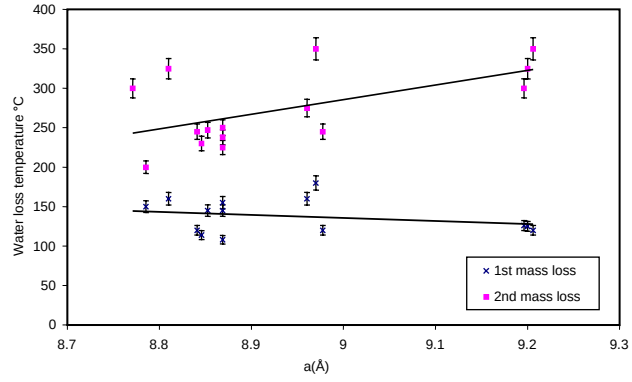

Fig. 8. Change in water loss temperature with cell parameter (a).

potassium-exchanged hydrosodalite there are two distinct temperatures ranges (100–200°C, 250–350°C). Presumably, two factors affect the loss of water from the cage. As the first water loss is higher for the smaller cations, it suggests that the smaller, more polarizing cations hold the water molecules more tightly in the first instance. However, once the first four water molecules are lost it is likely that the dominant factor affecting the water loss is the size of the metal cation; since the larger cations appear to facilitate a higher water loss temperature. It appears likely that as the metal cation resides in the six-ring window, it can block the path of the exiting water molecules. The larger cations are therefore more effective at blocking the path leading to a higher temperature of water loss.

In situ powder X-ray diffraction was performed on the samples between room temperature and 1000°C. All ion-exchanged hydrosodalites exhibit a clear phase change between 200°C and 300°C, while two phase changes are apparent in systems with larger cell parameters. The changes can be noted by the difference in peak intensities and the cell size. An example of the X-ray diffraction profile for the in situ X-ray diffraction experiment for the potassium-exchanged hydrosodalite is given in Fig. 9. The first phase change to a system containing four water molecules occurs between 60°C and 250°C. Loss of four more water molecules occurs between 250°C and 350°C. Finally, above 900°C the phase starts to decompose to form nepheline, which is typical for sodalite systems.

3.4. Vibrational spectroscopy

The vibrational spectra of sodalite frameworks have been fully analyzed in detail by Creighton et al. [12]. For materials of the sodalite structure crystallizing in the space group $P\bar{4}3n$, 14 modes are infrared active in aluminosilicate derivates with ordered Si and Al. Intensity calculations show that nine of these vibrations, at frequencies up to 1200 cm^{-1}, are of reasonable intensity. However, generally, only five or six absorptions are readily resolved in the infrared spectrum, and these are a combination of asymmetric stretches near 950 cm^{-1} and three symmetric bands in the region 700–1000 cm^{-1} and one or two bending vibrations at lower frequency, typically 400–550 cm^{-1}. The frequencies of the stretches and bending vibrations have been shown to correlate with the sodalite a parameter and T–O–T' bond angle in a number of sodalite systems [13,14]. In agreement with previous studies, as the cell size increases in the ion exchanged hydrosodalite, the frequency for the symmetric stretches and deformations increase while for the asymmetric stretch the frequency falls (Fig. 10).

3.5. MASNMR

The Al^{27} and Si^{29} MASNMR (Figs. 11 and 12) spectra consist of a single sharp resonance in the case of the alkali metal exchanged hydrosodalite materials, while the calcium exchanged sample is significantly broadened. The resonances are centered at –90 ppm for

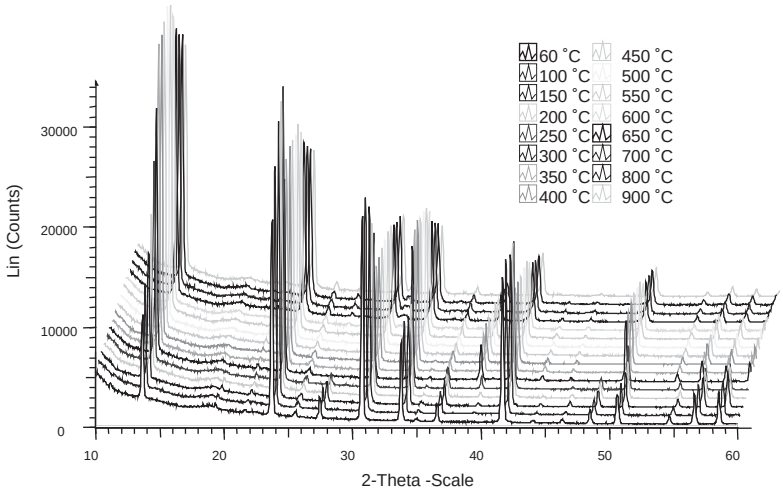

Fig. 9. High-temperature in situ X-ray diffraction study of potassium exchanged hydrosodalite.

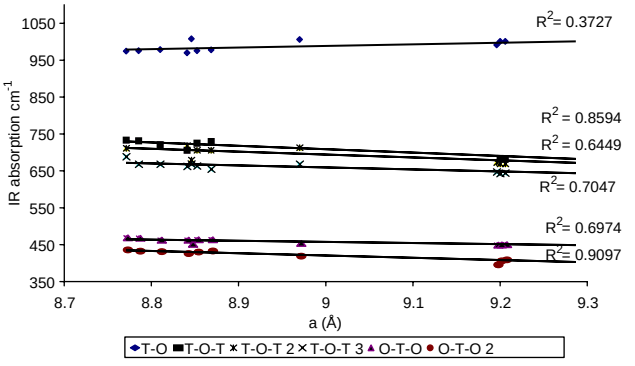

Fig. 10. Change in metal–oxygen bond stretching frequencies for hydrosodalite with cell parameter (a).

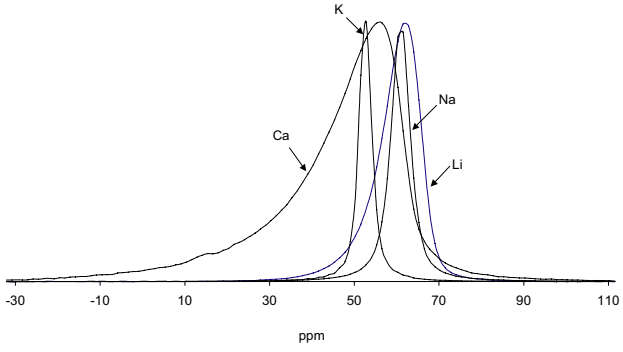

Fig. 11. ^{27}Al MASNMR data for ion exchanged hydrosodalite.

Si and 60 ppm for aluminum and are characteristic of tetrahedral silicon and aluminum, respectively, in an ordered sodalite framework structure [15]. The broadened resonance in the calcium-exchanged sample is most likely due to loss of crystallinity caused by damage to the framework during ion exchange. However, there is no sign of octahedral aluminum in the MASNMR (0 ppm).

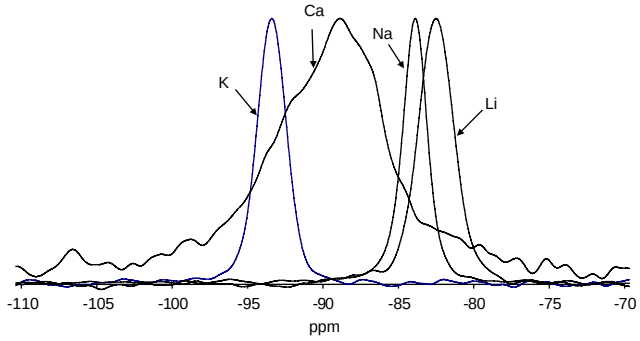

Fig. 12. ^{29}Si MASNMR data for ion exchanged hydrosodalite.

4. Conclusion

Alkali metal and alkali-earth metal hydrosodalites with the formula $M_6[AlSiO_4]_6 \cdot 8H_2O$ (M = Li, Na, K, Mg, Ca, Sr) have been prepared by ion exchange of $Na_6[AlSiO_4]_6 \cdot 8H_2O$. Occlusion of different metal cations within the sodalite framework affects the dehydration temperature such that the water molecules are lost in a two-stage process.

Supplementary Materials

Further details of the crystal structure investigations can be obtained from the Fachinformationszentrum Karlsruhe, 76344 Eggenstein-Leopoldshafen, Germany, (fax: +49-7247-808-666; e-mail: crysdata@fiz.karlsruhe.ed) on quoting the depository numbers CSD-413491-AL6 H16 NA1.2 CA2.4 O32 SI6; CSD-413492-AL6 H16 NA5.856 CS0.144 O32 SI6; CSD-413493-AL6 H16 NA5.656 CS0.344 O32 SI6; CSD-413494-AL6 H16 NA6 O32 SI6 $a = 8.8687$; CSD-413495-AL6 H16 NA6 O32 SI6 $a = 8.904$; CSD-413496 AL6 H16 NA8 O28 SI6; CSD-413497-AL6 H16 NA1.2 K4.8 O32 SI6 $a = 9.1786$; CSD-413498-AL6 H16 NA1.2 K4.8 O32 SI6 $a = 9.2060$;

CSD-413499-AL6 H16 NA0.21 K5.79 O32 SI6; CSD-413500-AL6 H16 NA3.3 Li2.7 O32 SI6; CSD-413501 -AL6 H16 NA3.728 LI2.272 O32 SI6; CSD-413502 -AL6 H16 NA6 O32 SI6; CSD-413503 -AL6 H16 NA1.056 SR2.472 O32 SI6.

Acknowledgments

We would like to thank Dr. David Apperley at the MASNMR service at the University of Durham for the solid state NMR data.

References

[1] V.G. Evsyunin, A.N. Sapozhnikov, R.K. Rastsvetaeva, A.A. Kashaev, Kristallografiya 41 (1996) 659–662.
[2] H. Schulz, H. Saalfeld, Miner Petrograph Mitt Tscher 10 (1965) 225–232.
[3] S. Werner, S. Barth, R. Jordan, H. Schulz, Zeit. Krist. 211 (1996) 158–162.
[4] B. Beagley, C.M.B. Henderson, D. Taylor, Miner. Mag. 46 (1982) 459–464.
[5] U. Simon, M.E. Franke, Micro. Meso. Mater. 41 (2000) 1–36.
[6] J. Felsche, S. Luger, Ch. Baerlocher, Zeolites 6 (1986) 367–372.
[7] S.E. Latturner, J. Sachleben, B.B. Iversen, J. Hanson, G.D. Stucky, J. Phys. Chem. B 103 (1999) 7135–7144.
[8] M.E. Brenchley, M.T. Weller, Zeolites 14 (1994) 682–686.
[9] I. Hassan, H.D. Grundy, Acta Crystallogr. C 39 (1983) 3–5.
[10] E. Kendrick, R. Morris, S.E. Dann, Solid State Phenom. 90–91 (2003) 57–62.
[11] A.C. Larson, R. Von Dreele, GSAS, LANSCE, MS-H805 Los Alamos National laboratory.
[12] J.A. Creighton, H.W. Deckman, J.M. Newsam, J. Phys. Chem. 98 (1994) 448–451.
[13] G.M. Johnson, P.J. Mead, M.T. Weller, Phys. Chem. Chem. Phys 1 (1999) 3709–3714.
[14] M.T. Weller, J. Chem. Soc. Dalton Trans. 23 (2000) 4227–4240.
[15] H.S. Jacobsen, P. Norby, H. Bildsoe, H.J. Jakobsen, Zeolites. 9 (1991) 1508–1513.